Optimal fibre architecture of soft-matrix ballistic laminates

Karthikeyan K[a], S. Kazemahvazi[a,b], B. P. Russell[a,*]

[a]*Engineering Department, University of Cambridge, Trumpington Street, Cambridge, CB2 1PZ, UK*

[b]*Department of Aeronautical and Vehicle Engineering, Kungliga Tekniska Högskolan, Teknikringen 8, Stockholm 100 44, Sweden*

[*]*Corresponding author: +44(0)1223 748541, bpr23@eng.cam.ac.uk*

Abstract

Soft-matrix ballistic laminates (such as those composed of fibres of Ultra High Molecular-Weight Polyethylene, e.g. Dyneema® HB26 and Spectra Shield), find extensive use as catching type armour systems. The relationship between the lay-up of these laminates with respect to the observed failure mechanisms has not been empirically investigated in the open literature, and is the subject of this work. Lay-ups are characterised by two parameters: (i) sequencing (or interply lay-up angle) $\bar{\theta}$ and (ii) in-plane anisotropy β, and can be mapped on to $\bar{\theta}$–β space. Four geometries that lie at the extrema of this parameter space are designed, built and tested. Testing is through ball bearing impact on circular clamped plates. The anisotropy (β) is coupled to the macroscopic response of the plates, whilst sequencing ($\bar{\theta}$) is coupled to the microscopic response. Penetration velocity is strongly affected by pull-out at the boundary, and in the present study this is shown to account for two-thirds of the ballistic resistance. The results have implications for validation testing on scaled samples, predictive modelling and simulation, and armour design.

Keywords: composite, laminates, ballistics, lay-up, fibres

1. Introduction

Light-weight ballistic armours are of key interest as protective systems against high velocity fragments, both for military application (protective vests) and civil use (turbine engine nacelles). At present, the best mass-efficient armours are polymer fibre based laminates. Ultra High Molecular-weight Polyethylene (UHMWPE) fibre laminates are one such armour system. They are of a class of composite materials that differs from more traditional structural composite systems (like carbon-fibre reinforced epoxies) in that they are significantly weaker in shear [1]. The combination of high fibre strength and low matrix shear strength results in a suite of complex mechanisms that gives rise to their unrivalled performance, and consequently, they see extensive use in military and civil protection. It is only recently that much of the underlying physics has been understood. Low shear strength enables large interlaminar and intralaminar shear strains [1, 2], increasing the structural compliance to allow out-of-plane displacement, and in so doing, reducing the peak pressures exerted by the projectile. The nature of the local failure of the fibres under the projectile has been the subject of some debate, but recent publications [3, 4] provide evidence for the so-called *indirect-tension* mechanism, whereby fibres fail in tension through the constraint imposed on lateral expansion by the orthogonal arrangement of plies. An important component of this mechanism is the pressure-dependent shear stress which has been demonstrated in these laminates [5].

The fibre architecture within a plate has a first-order effect on its ballistic limit; yet there is very little literature that explores this aspect. The ballistic capability of laminates with an orthogonal lay-up was recognised by inventors in the late 1940s [6, 7], and is still the architecture chosen for the latest fibrous armours [8].

Vargas-Gonzalez et al. [9], Vargas-Gonzalez and Gurganus [10], Zhang et al. [11] investigate a large number of lay-ups (orthogonal lay-ups, isotropic, and hybrids) and fibre types to assess both ballistic limit and back face deflection in relation to helmet design. Both parameters must be balanced to achieve acceptable survivability. Wang et al. [12] looked at the effect of multi-angled plies with woven fabrics, and report that multi-angled plies absorb more energy. Some studies using carbon fibre/epoxy composites have been performed on so-called helicoid lay-ups (e.g. [13, 14]). These showed an improvement in impact strength over more traditional quasi-isotropic lay-ups.

The gap in understanding is how fibre architecture relates to these assessment criteria (i.e. ballistic limit, back face deflection) with respect to the underlying mechanics; and consequently, what tools are required for the engineer to design configurations that maximise penetration resistance, back face deflection, or some combination of the two.

Presently, it shall be demonstrated how the lay-up architecture relates to a number of different deformation mechanisms that operate in polyethylene fibre laminates systems. In particular, the essential characterisation parameters of the laminate are defined that relate to the main mechanistic groups. Configurations are tested that explore the extremes of lay-up design. We then proceed to demonstrate where optimal lay-ups exist with respect to ballistic limit.

1.1. Macro and micro mechanism groups

The failure of UHMWPE laminates is complex, involving a range of interrelated mechanisms. The approach taken here is to categorise deformations into what shall be termed *macro mechanisms*: deformations that occur over the whole geometry, and *micro mechanisms*: deformations in the immediate vicinity of the projectile impact site, Fig. 1. The former encompass a group of interacting mechanisms: pull-out, interlaminar shear, intralaminar shear (or scissoring), and the latter: indirect tension and splitting. These two umbrella categories shall be considered throughout this paper.

We shall presently show how the laminate architecture influences both the macro and micro mechanisms, and how the overall ballistic performance arises from the contribution that each of these categories brings in the retardation of the projectile.

For clarity, splitting and indirect tension are defined at this point, since these terms are used to mean specific things throughout this study.

Splitting This is the transverse failure of a ply (or stack of plies) with respect to the fibre direction, Fig. 1d. The strength is governed by the matrix tensile strength and the interfacial strength between fibre and matrix. Fibres themselves are not fractured, rather they are pushed laterally with respect to the projectile trajectory to allow passage of the projectile.

Indirect tension Fibre-failure within a 0°/90° lay-up under the projectile has been extensively investigated and modelled [3, 4, 15]. Failure of fibres is through tension, which arises from the mutual constraint imposed on the Poisson's expansion from the alternating 0° and 90° plies. An important component is the pressure-dependent shear strength that prevents splitting. Note here that the deformation around the region of indirect-tension is complex and involves transverse ply failure, see detailed micro XCT of O'Masta et al. [4]. However, the term 'splitting' is reserved to indicate situations where transverse ply failure is the primary mechanism by which penetration is achieved.

1.2. Characterisation of architectures

Limiting the scope of architectures to 2D, non-woven systems, fibre lay-ups can be quantified in terms of their *anisotropic ratio* and *sequencing*. These quantities can be defined as follows:

Anisotropic ratio The range of different ply angles in a lay-up will have a bearing on the variation of the in-plane stiffness, Fig. 2. Extreme anisotropy is seen in unidirectional long-fibre composites, where the longitudinal stiffness is often orders of magnitude greater than the transverse stiffness. The anisotropic ratio, β is defined thus:

$$\beta = \frac{E_{\max} - E_{\min}}{E_{\max}} \tag{1}$$

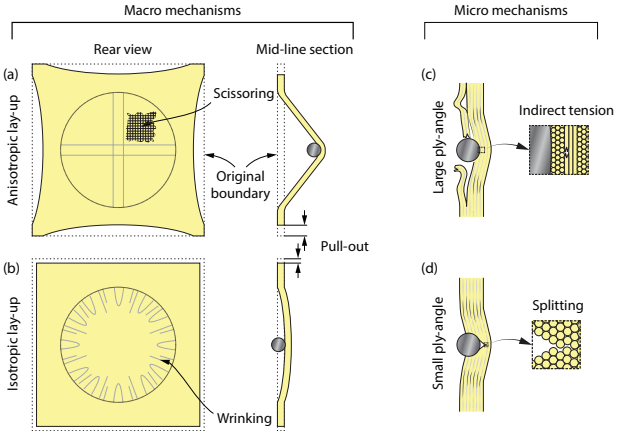

Figure 1: Overview of the deformation mechanisms of UHMWPE laminates. Macro mechanisms differ between (a) anisotropic and (b) isotropic lay-ups. In the first case, pull-out is large and scissoring occurs; in the latter, pull-out is small and wrinkling is seen. Micro mechanisms operating under the projectile are either (c) fibre-failure through indirect-tension, which is associated with large ply off-set angles, and (d) splitting, occurring at small angle off-sets.

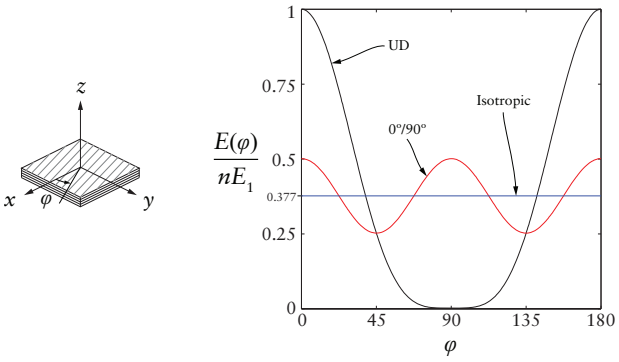

Figure 2: Plot of the variation of in-plane stiffness as a function of the in-plane angle, ϕ, for unidirectional (UD), 0°/90° and isotropic lay-ups. This is normalised by the stiffness along the fibre direction of a single ply (E_1) and the number of plies in the laminate (n). Typical values for a UHMWPE ply are used. Note that the extreme anisotropy in a ply ($E_1 > E_2, G_{12}$ by 3 orders of magnitude) causes this plot to be relatively insensitive to exact ply values.

Where $E_{\max}$ and $E_{\min}$ are the maximum and minimum stiffnesses in the plane of the laminate. In the case of a UD lay-up: $\beta \sim 1$, and an isotropic lay-up would give: $\beta = 0$.

Sequencing The angle between fibres of adjacent plies, θ, influences how plies interact with each other. The average of θ through the composite needs to take into account the ordering of plies through the whole laminate. Given that θ is not necessarily constant through the laminate, it is convenient to define an averaged quantity, $\bar{\theta}$:

$$\bar{\theta} = \frac{1}{k\,(n-1)} \sum_{i=1}^{n-1} |\theta_{i+1} - \theta_i| \qquad (2)$$

Where n is the number of plies in the lay-up, and k is the angle of a right-angle (i.e. 90°), providing a normalisation such that $\bar{\theta}$ lies between the limits of 0 and 1.

Any particular lay-up will exist at a single point in $\bar{\theta}$–β space; however, any particular point in this space may correspond to more than one lay-up. While aspects of the laminate such as ply thickness are not captured by this methodology, the intention of this work is to focus on the arrangement of fibre orientations.

1.3. Choice of architectures

Four fibre architectural arrangements are considered in the present study: unidirectional (UD), alternating orthogonal (0°/90°), helicoidal and lastly, a hybridised 0°/90°–Helicoid arrangement. The exact architectures of the lay-ups are given in Fig. 3.

Since both β and $\bar{\theta}$ are bounded quantities, all combinations of ply arrangement can be mapped into $\bar{\theta}$–β space, Fig. 4. The region marked *unattainable space* describes combinations of $\bar{\theta}$ and β that cannot exist. Consider the two lay-ups on this boundary: to increase $\bar{\theta}$ from the UD coordinate would necessarily cause β to decrease by introduction of new fibre directions; to increase β from the 0°/90° coordinate either the ratio of 0°:90° must be changed (resulting in adjacent plies of the same fibre orientation), or the angle between plies must decrease, both leading to a decrease of $\bar{\theta}$.

The particular choice of the four lay-ups of Fig. 3 allows us to explore the corners of this space. Thus the selection of different pairs allow us to compare each parameter in turn. For example, the 0°/90° and the 0°/90°–

Stack	θ	Lay-up
UD	0°	$[0°]_{48}$
0°/90°	90°	$[0°/90°]_{24}$
Helicoid	3.75°	[0°/3.75°/7.5°/.../176.25°]
0°/90° – Helicoid	15°	$[(0°/90°)_2/(15°/-75°)_2/.../(-15°/75°)_2]$

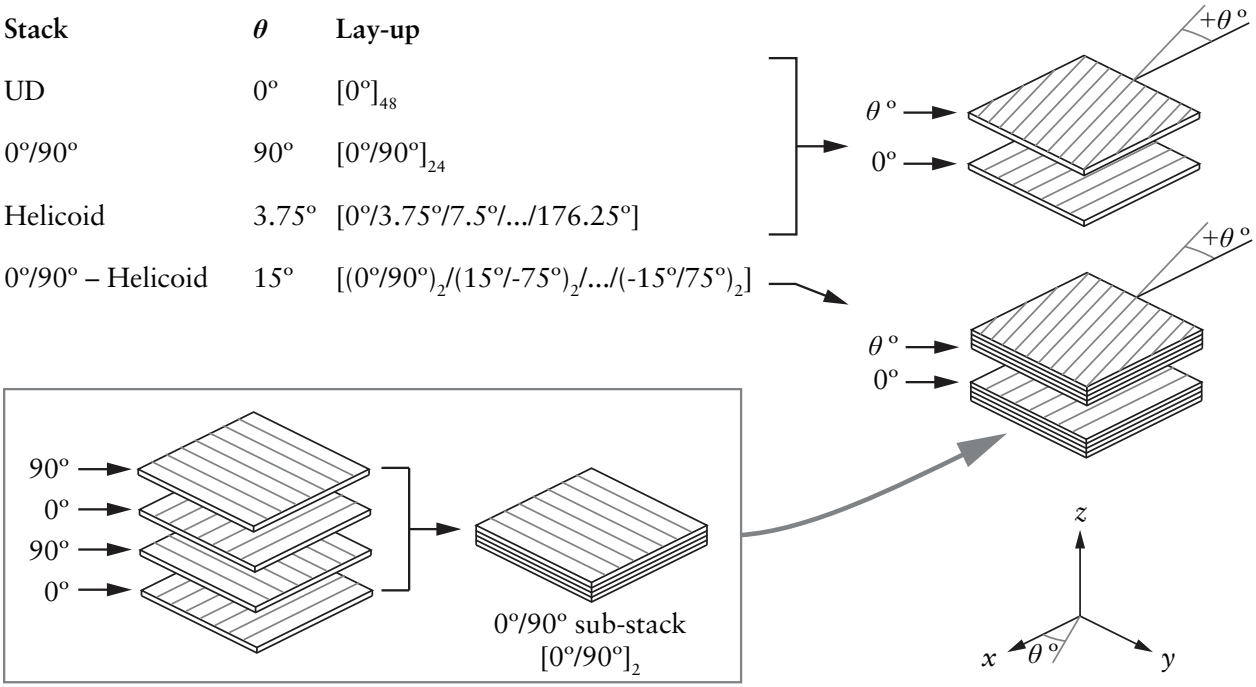

Figure 3: Lay-ups used for the laminates in this study. Note that the UD and 0°/90° lay-ups can be considered special cases of the helicoid geometry with θ values of 0° and 90° respectively. The 0°/90°– Helicoid is arranged in a similar fashion, but in this case, blocks of orthogonal plies are arranged in a helicoidal manner.

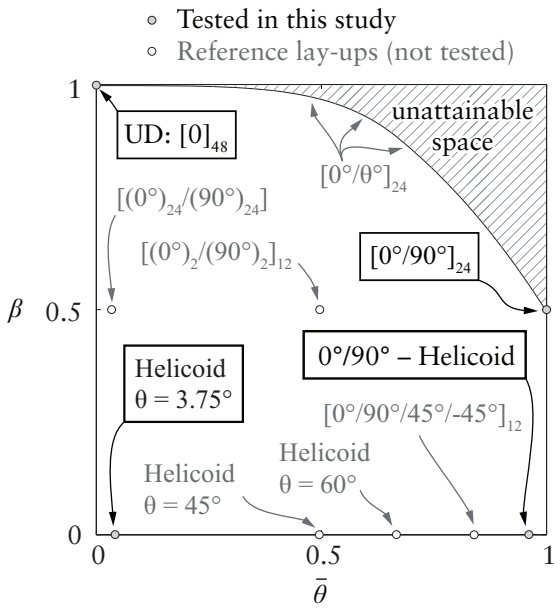

Figure 4: Map of $\bar{\theta}$–β space showing the location of each of the four lay-ups. The region marked 'unattainable space' excludes impossible lay-ups, the boundary is constructed by calculating $\bar{\theta}$ and β for lay-ups that have 2 fibre directions with half the plies orientated at 0° and the other half at some angle θ between 0° and 90°. The four lay-ups investigated in this study are shown boxed. For reference, the positions of other lay-ups are given, e.g. quasi-istotropic: $[0°/90°/45°/-45°]_{12}$.

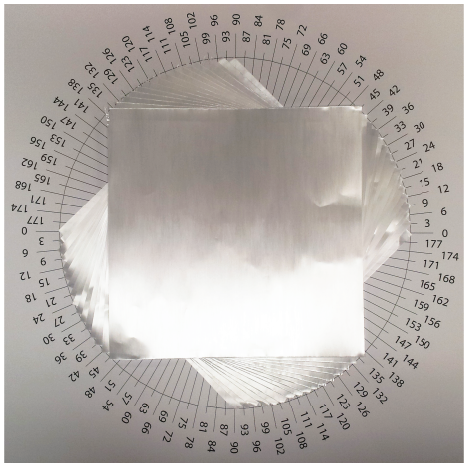

Figure 5: Construction of the helicoid geometry using a 'compass' guide. Square sheets with side length 212 mm (= $\sqrt{2} \times 150$ mm) are positioned such that two diametrically opposite corners are located at the antipodal increment marks.

Helicoid pairing allows us to change β whilst maintaining similar $\bar{\theta}$.

2. Materials and methods

2.1. Laminate material and lay-up

A roll of single ply Ultra High Molecular-Weight Polyethylene (UHMWPE) fibres with a polyetherdiol-aliphatic diisocyanate polyurethane (PADP) matrix was supplied by DSM Dyneema.[1] This precursor is used in the production of laminates with commercial designation HB26. The fibre type is designated SK76 and constitutes 0.83 of the total volume of the composite, with the polyurethane matrix making up the remainder. The mechanical properties of the fibre and 0°/90° laminate material have been characterised previously and are not reported here for brevity [1, 16]. The precursor and the derived laminates have a density $\rho_t = 970$ kg m^{-3}.

Figure 3 shows details of the four lay-ups. The unidirectional and 0°/90° laminates are straightforward to construct. However, the helicoid geometries require some careful placement. In order to facilitate the precise positioning of each ply, a 'compass' guide was created with increments of the desired θ, Fig. 5. This procedure ensured that placement error was within ±1.5°. The overlap area of the plies was a circle of ⌀212 mm. All lay-ups consisted of a total of 48 plies.

The consolidation protocol was carried out using a *Fontijne Press*[2]. Although this protocol was identical for all lay-ups (see Table 1), some special handling was required for the UD. The UD material is highly compliant perpendicular to the fibre direction so a steel encasement, within which the laminate was pressed, ensured a plate width of 150 mm and prevented lateral extrusion. Post-

[1] DSM Dyneema B.V., Mauritslaan 49, 6129 EL Urmond, The Netherlands.

[2] Manufactured by Fontijne Grotnes Hydraulic Laboratory, Industrieweg 21, 3133 EE Vlaardingen, Netherlands. Platen Press Code number: LPC 043.

Table 1: Consolidation cycle used in the production of laminates.

Phase	Duration (min)	Temperature (°C)	Pressure (MPa)
Pre-heat	10	90	–
Ramp up	7	90-127	20
Hold	20	127	20
Ramp down	7	127-90	20

consolidation, helicoid specimens were sandwiched between wooden boards and cut to 150 × 150 mm squares using a bandsaw.

2.2. Ballistic test protocol

The experimental set-up is sketched in Fig. 6, and follows a similar method used in previous studies [17, 18]. Chrome steel spheres[3] (AISI 52100) of diameter 12.7 mm and mass 8.3 g were accelerated at plates, using a gas-gun of barrel length 4.5 m and bore diameter 13 mm. These projectiles impacted the test plates centrally and normally (zero obliquity). The velocity of projectiles was measured at the gun muzzle by a set of laser gates. The velocities V of the present study ranged from 75 m s^{-1}to 500 m s^{-1}.

2.3. Specimen boundary condition

Test plates measured L = 150 mm × 150 mm and were clamped between two steel plates, each with a circular cut-out of ⌀100 mm. Eight equi-spaced M10 bolts situated on a 90 mm pitch radius from the plate centre, were torqued to 40 Nm translating to approximately 91 - 160 kN of clamping force. This force was distributed over an area of 48 cm^2 giving an average clamping pressure of 19 - 33 MPa. A torque wrench was used to ensure an even and repeatable pressure. Bolts were tightened incrementally and in order (as per the numbering shown in Fig. 6).

3. Results and observations

3.1. Ballistic performance

The ballistic limit velocities V_L for the four lay-ups (Fig. 3) are shown in Fig. 7a. The V_L is defined to be the mean of the lowest penetrating velocity and the highest surviving velocity. As might be expected, the UD material fails at the lowest velocity V_L = 108 ± 16 m s^{-1}, and is closely followed by the helicoidal lay-up at 138 ± 36 m s^{-1}. The high $\bar{\theta}$ lay-ups perform much better, with the 0°/90°– Helicoid and 0°/90° lay-ups obtaining 257 ± 13 m s^{-1}and 448 ± 13 m s^{-1} respectively. Table 2 lists all ballistic tests conducted for the study and is included for completeness.

Table 2: Summary of ballistic tests carried out on each lay-up type.

Lay-up	V_0 (m s^{-1})	Survival/Failure
UD	48	Survival
UD	92	Survival
UD	124	Failure
UD	490	Failure
Helicoid	103	Survival
Helicoid	174	Failure
Helicoid	245	Failure
Helicoid	365	Failure
Helicoid	420	Failure
Helicoid	448	Failure
Helicoid	485	Failure
0°/90°– Helicoid	244	Survival
0°/90°– Helicoid	270	Failure
0°/90°– Helicoid	286	Failure
0°/90°– Helicoid	345	Failure
0°/90°– Helicoid	466	Failure
0°/90°	400	Survival
0°/90°	435	Survival
0°/90°	460	Failure
0°/90°	473	Failure

However, it is only when lay-ups are compared in terms of the projectile kinetic energy that the relative performance of each lay-up is appreciated, Fig. 7b. Comparing performance on this basis, the 0°/90° lay-up withstands 3 times the projectile kinetic energy of the next best lay-up (the 0°/90°– Helicoid). In order to understand these dramatic differences in performance, we proceed to look at the mechanisms operating in each case, and subsequently, how these are determined by the choice of fibre architecture.

3.2. Observations of failure mechanics

Deduction of the mechanisms of deformation is made through (1) real-time observation of the deformation via high speed photography (Fig. 8), and (2) post-impact inspection of plates through direct observation and X-ray

[3]Chrome steel, AISI 52100. Obtained from Atlas Ball and Bearing Company Ltd., Leamore Lane, Walsall, England, WS2 7DE, UK.

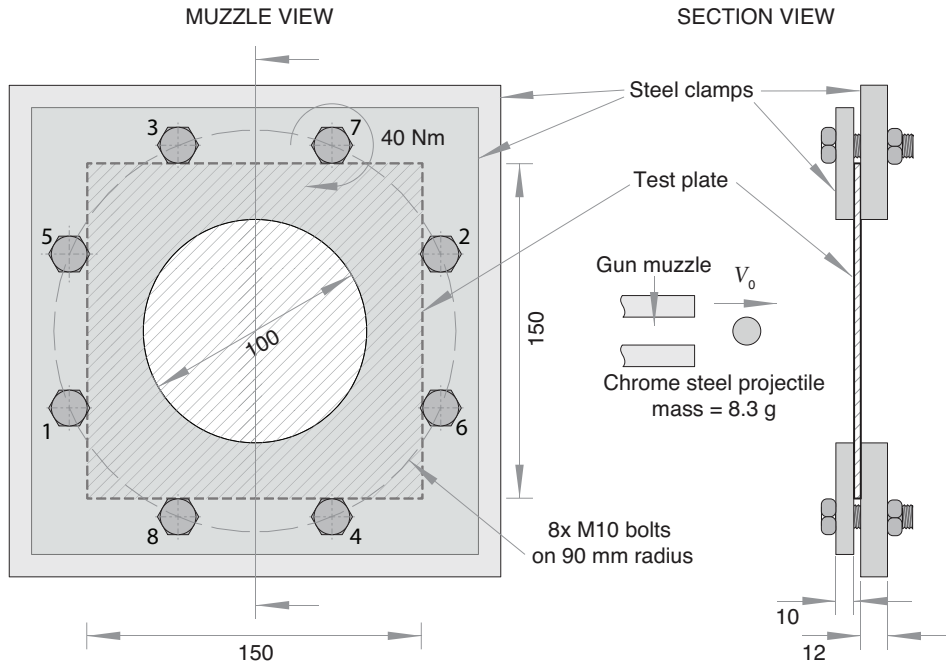

Figure 6: Experimental set-up showing (a) muzzle view of clamping fixture, and (b) a section view showing projectile trajectory. The test specimen is shown hatched. Numbers next to bolts indicate tightening sequence.

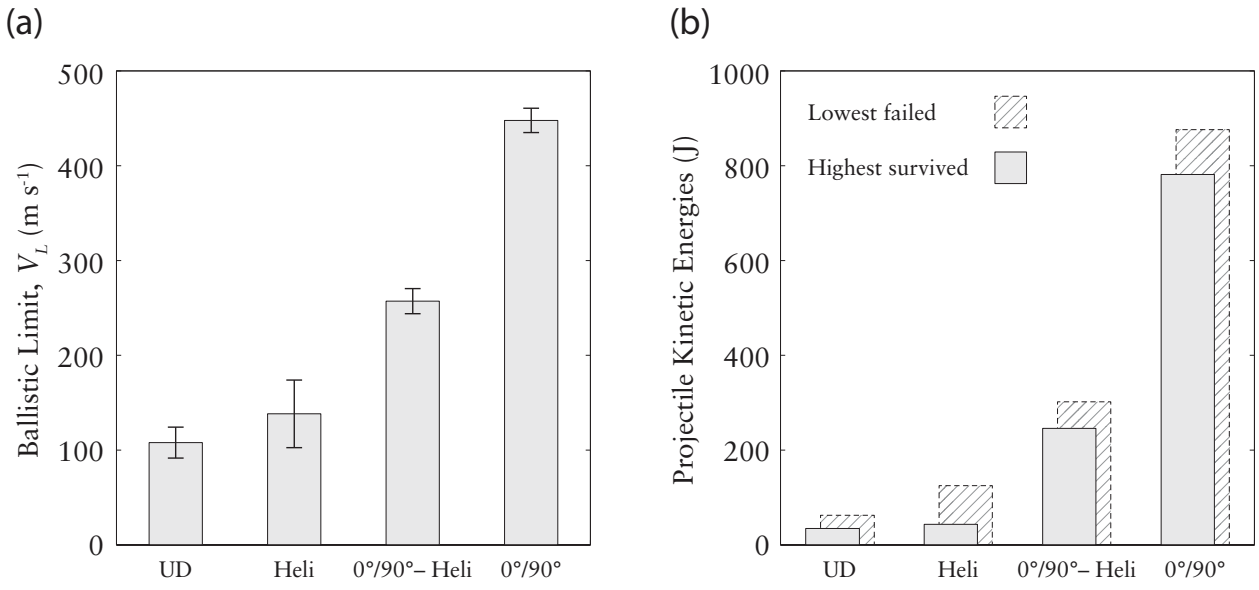

Figure 7: Comparison of the four lay-ups in terms of (a) ballistic limit V_L, and (b) kinetic energy of projectile for tests either side of the V_L. Upper and lower bounds of the error bars show the lowest penetrating velocity and the highest surviving velocity respectively.

computed tomography (Figs. 9, 10, 11, and 12). The deformation of each laminate is described as follows:

Unidirectional Deformation in the plate is limited to a strip of width 10 mm, running along the fibre direction, up to the plate edge. A large amount of pull-out is observed, facilitating the deflection of this central strip. No fibre failure is observed (this is also true for impacts at very high velocity $V = 490$ m s^{-1}), rather the passage of the projectile is permitted through the formation of a shear plugging feature, which arises through a combination of through-thickness shear and pull-out. Incipient splitting is observed in the contact region between projectile and plate. Splitting is defined as the transverse failure of a ply (or stack of plies) with respect to the fibre direction, Fig. 1d. The strength is governed by the matrix tensile strength and the interfacial strength between fibre and matrix. Fibres themselves are not fractured, rather they are pushed laterally with respect to the projectile trajectory to allow passage of the projectile. For the geometries tested at impacts just above the V_L, the central strip completely pulled out from the boundary before the projectile could pass through the plate by splitting (failure is through macro mechanisms rather than micro). At high velocity ($V = 490$ m s^{-1}), the projectile completely split the plate before pulling out the strip from the boundary. The procedure used to lay-up the UD configuration ensured that the maximum deviation of fibres from the 0° orientation was < 1°; even so, significant bridging is observed, Fig. 9.

Helicoid The extent of pull-out and therefore deflection is considerably less than either the 0°/90° or UD lay-ups. The distribution of the pull-out is also more uniform around the boundary. In terms of the micro mechanisms that are operating, this is the only one of the four lay-ups considered that shows both indirect tension and splitting, Fig. 10. At the V_L, approximately half of the plies fail by each mechanism. At high velocity ($V = 448$ m s^{-1}) the fraction of plies failing by indirect tension increases to about two-thirds. The initial deflection is also distinct from other lay-ups in that a 180° rotational symmetry is seen rather than the typical mirror symmetry of 0°/90° laminate. This is attributed to the differing levels of engagement of fibres at different depths in the lay-up, and is confirmed through a noticeable rotation of the bulge shape as deflection progresses. A single large delamination develops within the laminate. This is most clearly seen in impacts below the ballistic limit, Fig. 11.

0°/90°– Helicoid Similar to the Helicoid, very little pull-out is observed, and this is distributed uniformly around the boundary. Indirect tension is the only micro mechanism that permits passage of the projectile through the plate, Fig. 12a (this is the same micro mechanism seen in the 0°/90° lay-up, 12b). Initial deflection appears approximately pyramidal, and the edges of the pyramid align with the rear-most orthogonal plies, Fig. 8. The pyramid is not perfectly mirror-symmetric, having a slight rotational symmetry arising from the engagement of the other $[0°/90°]_2$ blocks towards the distal face. At larger deflections, the shape is no longer pyramidal but domed and wrinkling is seen towards the edges of the plate as the pyramid approaches the boundary.

0°/90° Cross-ply Pull-out occurs to a large extent and is at a maximum where fibres directly intersect the impact site (Fig. 8, particularly B to D). Fibre-fracture is the only micro mechanism that permits passage of the projectile through the plate. Initial deflection is pyramidal in shape, having 2-fold mirror-symmetry (Fig. 8A–B). Scissoring (rotation of one fibre layer with respect to another) occurs on the four facets of the pyramid.

4. Macro/Micro mechanisms relationship to β and $\bar{\theta}$

A summary of the macro and micro mechanisms, and the laminate architecture parameters (β and $\bar{\theta}$), for each laminate is given in Table 3. The β parameter is associated with the lay-up's propensity for pull-out and deflection, whilst the $\bar{\theta}$ parameter is related to the predominant mechanism by which the projectile locally fails the successive layers of the laminate: low and high $\bar{\theta}$ are correlated to splitting and fibre-fracture respectively. The following subsections proceed to an explanation of how each of the architectural parameters are linked to the resultant mechanics.

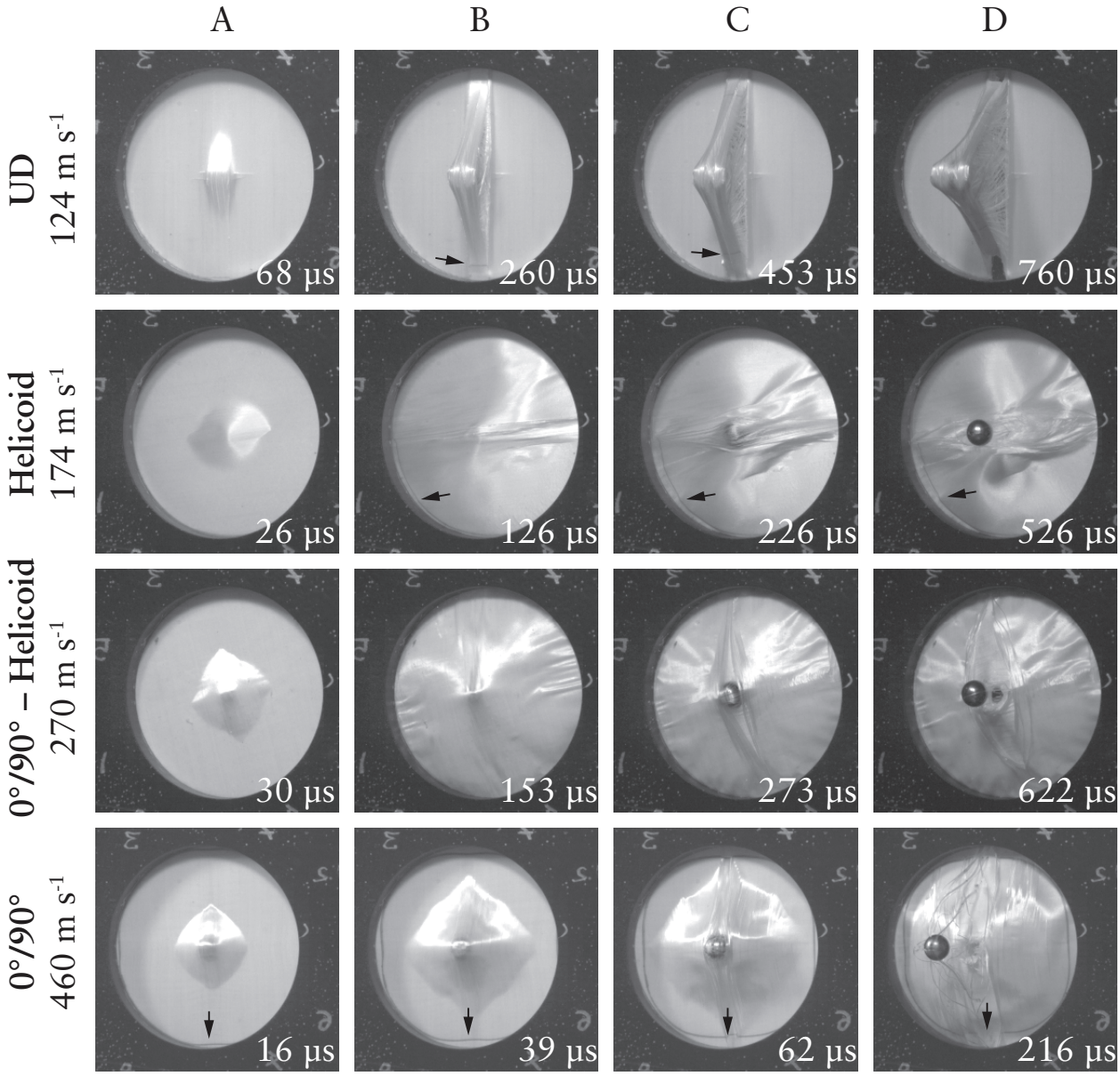

Figure 8: Montage of selected high-speed images for each of the four lay-ups for velocities just above the V_L. **A** shows the early stage deflection, and **C** shows incipient failure with **B** at an intermediate frame between **A** and **C**. **D** shows the plate after failure. Evidence of pull-out can be seen by the motion of the line drawn at the boundary, arrows marked on images to indicate the boundary.

Table 3: Summary table showing the observed mechanisms for each laminate.

Mechanisms →	Macro				Micro		Parameters	
	Pull-out	***Deflection***	***Delamination***	***Membrane***	***Fibre-failure***	***Splitting***	β	$\bar{\theta}$
UD	major	large (strip)	none	–	no	yes	1	0
Helicoid	minor	small	single	distortion	yes	yes	0	0.04
0°/90°– Helicoid	minor	small	significant	wrinkling	yes	no	0	0.96
0°/90°	major	large	significant	scissoring	yes	no	0.5	1

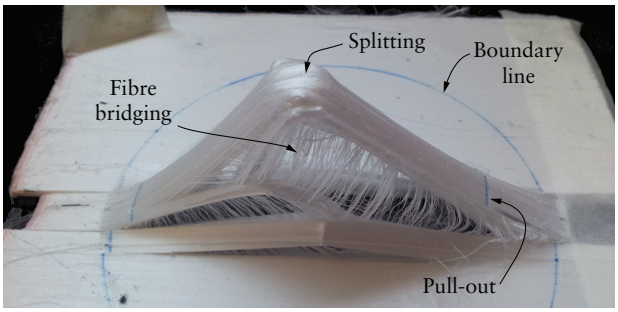

Figure 9: Rear face of UD plate after impact at $V = 90$ m s^{-1}. The extent of pull-out can be seen by the movement of the boundary line. Significant fibre bridging occurs; this is thought to be due to fibre mobility during the consolidation process.

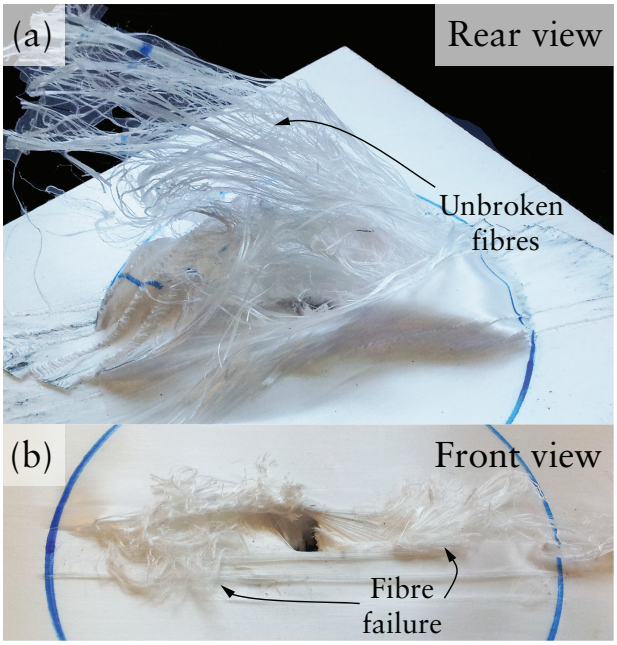

Figure 10: Close up images of the Helicoid (a) front and (b) rear faces. Note that fibre failure can be seen in (a) but not in (b).

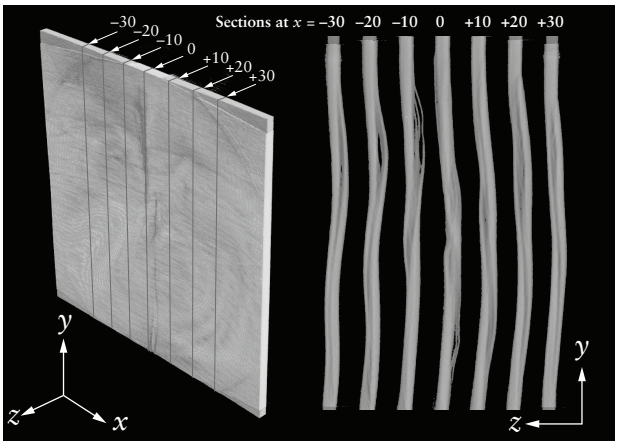

Figure 11: X-ray tomographic image of plate with helicoid lay-up after impact at 103 m s^{-1} (left) showing the presence of a helicoid delamination, visible through the sections (right). Section dimensions are in mm.

4.1. Macro mechanisms and the β parameter

Comparison of the 0°/90°– Helicoid and 0°/90° laminates allows us to consider the effect of β whilst keeping $\bar{\theta}$ approximately the same. The most notable difference between these lay-ups is that of deflection. Large deflections are associated with better ballistic resistance [9], and it will be shown how this arises from energy dissipation mechanisms through the two macro mechanisms of pull-out and in-plane shear resistance. The contributions of these mechanisms to the deflection is discussed in the following sections.

4.1.1. Pull-out

At the point of impact, longitudinal stress waves are generated and propagate along the so-called *primary fibres*. The primary fibres are those that lie underneath the projectile, Fig. 13. This band of fibres has a width $w = 8$ mm (in the 0°/90° lay-up, in the UD $w = 10$ mm) and

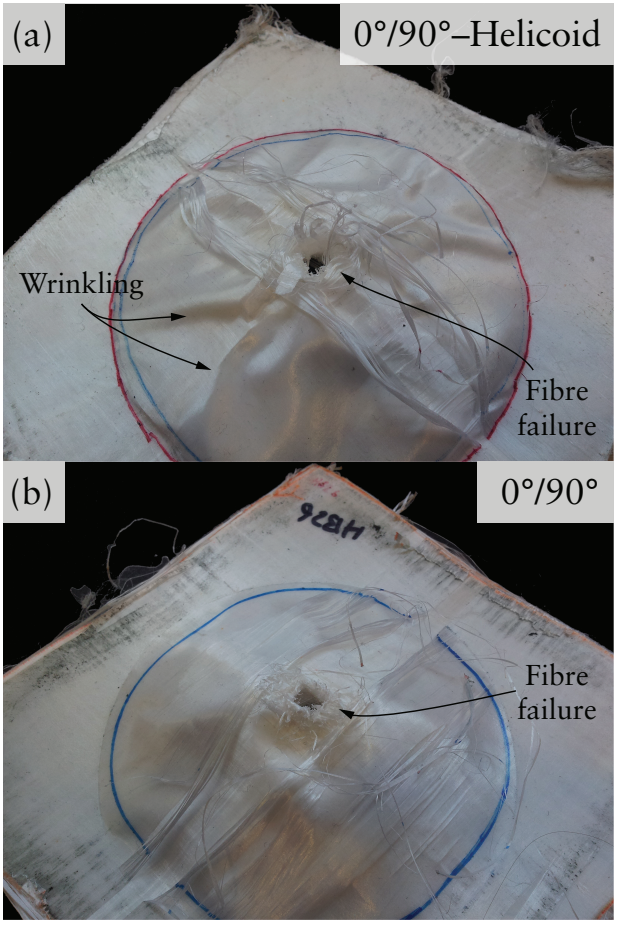

Figure 12: Post-impact rear face images of (a) 0°/90°– Helicoid and (b) 0°/90°– Helicoid plates. Note that fibre failure is very similar, but the macro deformations are distinct: (a) shows a dome with wrinkling, and (b) a squarish pyramid shape with smooth sides.

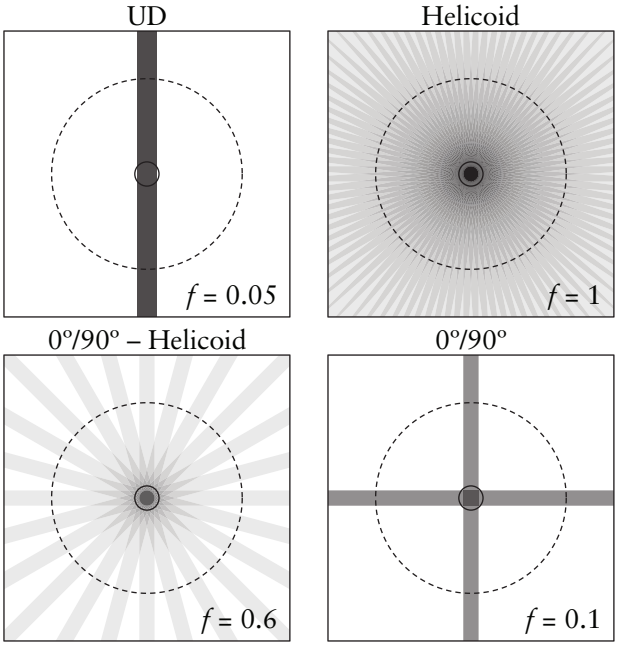

Figure 13: Schematics for each plate lay-up with the primary fibres shaded. Numeric values indicate the fraction of the boundary that is intersected by the primary fibres. Central circle shows the projectile, and the dashed line represents the position of the clamped boundary. The fraction of the boundary intersected by the primary fibres, f, is shown.

lies along the plate diameter. On reaching the plate edge, these waves are reflected at the free-end of the fibres and effect pull-out: drawing material in towards the impact site. This extra lengthening within the span permits deflection beyond that facilitated by the strain in the fibre, allowing large deflections.

For pull-out to be initiated, the frictional force F_F acting on the plate from the boundary clamps must be overcome by the load in the primary fibres F_B. The arrangement of these primary fibres (i.e. the anisotropy, β) has a direct bearing on the force distribution acting upon the boundary. F_B is inversely related to the fraction of the boundary that intersects with the primary fibres (f values in Fig. 13). In the 0°/90° arrangement (β= 0.5) the primary fibres are restricted to two directions (f = 0.1): load is focused at the four regions where these intersect the clamped boundary. In the case of the 0°/90°– Helicoid, the primary fibres engage with nearly two-thirds of boundary circumference.

To predict if pull-out is likely to occur for a given lay-up, the approximate fictional traction, F_F is first calculated at the boundary from the bolt torque and clamp geometry,

$$F_F = \mu_{sp}\left[n\,\frac{T}{\mu_{gzt}D}\right] \tag{3}$$

Where T and D are the bolt torque and nominal diameter, n is the number of bolts, and μ_{gzt} and μ_{sp} are the frictional coefficients for galvanised steel threads and steel-on-polyethylene respectively. This gives a value of $F_F = 3.7 - 6.4$ kN for the clamping arrangement in Fig. 6 ($T = 40$ N m, $D = 10$ mm, $n = 8$, $\mu_{gzt} = 0.275 \pm 0.075$ [19], $\mu_{sp} = 0.04$ [20]).

Next the maximum permissible load applied to a portion of the boundary is estimated. It is assumed that the maximum stress in the ply is its failure strength $\sigma_f = 1.7$ GPa and the laminate has a volume fraction of fibres of $V_f = 0.83$ [16]. The maximum permissible load on the boundary, F_B is:

$$F_B = \sigma_f V_f n_p t_{ply} w \tag{4}$$

Where t_{ply} is the ply thickness and w the width of the primary fibre band. The values are constant for all laminates with $t_{ply} = 60$ µm and $w = 8$ mm. n_p is the number of plies for which the primary fibres are engaged in one particular direction, and is related to f thus:

$$f = \frac{n_T}{n_p}\frac{w}{\pi R} \tag{5}$$

n_T is the total number of plies in the laminate. n_p varies with β, so is different for the 0°/90° and 0°/90°– Helicoid laminates. In the 0°/90° laminate half the plies in the laminate are in alignment with each other, whilst in the 0°/90°– Helicoid only two plies are in alignment. Thus the peak forces acting on the boundary in the 0°/90° and 0°/90°– Helicoid cases are $F_B = 16$ kN and 1.4 kN respectively.

For the 0°/90° lay-up, $F_B > F_F$, indicating that pull-out will likely occur, and is in agreement with experimental observations. In the case of the 0°/90°– Helicoid, $F_B < F_F$, suggesting no pull-out, which again matches what is observed experimentally. This difference in pull-out is the main discrepancy between these lay-ups (Table 3), and thus is the key factor that results in the superior ballistic performance of the 0°/90° plate (refer to Fig. 7). An estimate can be made of the contribution to ballistic resistance by accounting for the work done in pull-out. The energy dissipated in overcoming friction at the boundary, U_{PO} is simply given as the product of the frictional resistive force F_F from Equation 3 and the average pull-out, $\bar{d}$:

$$U_{PO} = F_F \bar{d} \tag{6}$$

The average pull-out $\bar{d}$ of the 0°/90° plate is calculated for two velocities, $V = 400$ m s^{-1} and 460 m s^{-1}, which lie either side of the V_L ($\bar{d} = 20$ mm and 4.2 mm respectively). The work done in pull-out is 340 J and 70 J, and account for 50% and 8% of the initial projectile kinetic energy. For the 0°/90°– Helicoid lay-ups, $\bar{d} = 2$ mm for impacts either side of the V_L ($V = 245$ m s^{-1} and 270 m s^{-1}). The contribution of U_{PO} in the survived 0°/90° plate correlates well with the additional kinetic energy dissipated over that of the 0°/90°– Helicoid plate.

4.1.2. In-plane shear

A second effect that arises from anisotropy is that of the in-plane shear stiffness and strength. The in-plane shear response is important since some distortion is required to move from a planar surface to one with a positive Gaussian curvature. To facilitate this morphological transformation, either stretching or folding is necessary.

From laminate plate theory, the value of G_{xy} is probed as function of ϕ for the 0°/90° and 0°/90°– Helicoid lay-ups in the same way as for the direct stiffness, E in Fig. 2. G_{xy} is inversely proportional to E, so for the 0°/90° case low stiffness directions are observed, whilst in the 0°/90°– Helicoid case G_{xy} is constant.

Mechanistically, the reason for this can be explained via analogy with Maxwell's work on frames [21]. When an in-plane shear strain is imposed through some loading, it is no longer possible for fibres to maintain their original orientation with respect to each other. When the number of unique fibre directions equals 2, shear can be accommodated without need to impose deformation on the fibres Fig. 14a–b. Thus the 0°/90° lay-up exhibits an intralaminar shear or 'scissoring' mechanism in which only the matrix contributes resistance. In contrast, in any structure possessing 3 or more unique fibre directions, some sort of

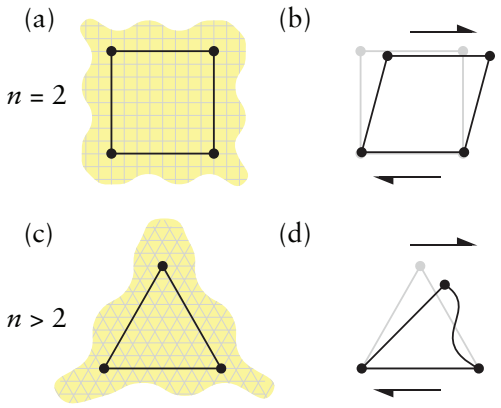

Figure 14: For lay-ups where $n = 2$ (a), fibre architecture will behave as a mechanism under a shear load, with no fibre deformation (b). Where $n > 2$ (c), fibre architecture will behave like a structure and fibre deformation is required to accommodate deformations under shear (d).

triangulation of the structure will result, such that the fibres themselves must undergo distortion to accommodate a shear strain, Fig. 14c–d. Shear is inhibited as the third direction acts to oppose the scissoring action of the first two. In the 0°/90°– Helicoid lay-up, multiple fibre directions are present, thus fibres also contribute resistance to deformation. Out-of-plane deflection results in wrinkling around the periphery of the deflected region.

In contrast to the 0°/90°– Helicoid lay-up, the out-of-plane motion is less inhibited in the 0°/90° lay-up where the mechanism of pull-out and intralaminar shear work together as a pair to facilitate deflection. The ease with which shearing occurs is a key enabler that aids pull-out, which dissipates significant energy. However, the contribution to dissipation from intralaminar shear itself is likely to be much less significant than that of pull-out, since the shear stress is so low. The rate dependence and effect of pressure are unknown and is an area where further research is required.

4.2. Micro mechanisms and the $\bar{\theta}$ parameter

Comparison of the Helicoid and 0°/90°– Helicoid pair of laminates (and the UD and 0°/90° pairing) allows us to consider the effect of $\bar{\theta}$ whilst keeping β approximately the same. The key architectural difference between these lay-ups is the introduction of adjacent orthogonal layers, which increases $\bar{\theta}$ dramatically whilst preserving isotropy (in the case of the helicoids).

High $\bar{\theta}$ lay-ups exhibit only indirect tension failure. It seems that the presence of orthogonal plies completely switches off the splitting mechanism (although transverse ply failure is seen outside the central region failed through indirect tension).

$\bar{\theta} = 0$ implies a single fibre orientation, and in this case, splitting is the only micro mechanism available that permits passage of the projectile through the plate.

The helicoid lay-up is a special case as both fibre-failure and splitting are observed for the same fibre arrangement, i.e. an inter-ply angular off-set of 3.75°. What is it that governs the transition between these two mechanisms? Under impact, the front of the plate will experience the largest pressure. It appears as if the initial pressure is sufficient to elevate the shear strength to the point of fibre-failure. Subsequently, as momentum is transferred to the plate, the pressure reduces, and splitting now operates as the failure mode. This is consistent with the observation that the fraction of the plate that fails through fibre-fracture increases with impact velocity. The authors speculate that this transition would occur at earlier velocities as the angular off-set is increased (assuming no change to overall plate compliance).

At present, the dependency of this pressure-dependent shear strength on the in-plane stress state is not fully understood and merits further investigation.

4.2.1. High velocity impact

For a given plate architecture, the interplay between the macro and micro mechanisms is determined by the velocity of the projectile. The time available for mechanistic interaction is inversely related to the projectile velocity, and since the characteristic lengths for these mechanism categories differ by 3 orders of magnitude, it follows that the dissipative contributions from the macro mechanisms will decrease at higher and higher impact velocities.

An additional set of impact tests were performed at high velocity, between 450 to 490 m s^{-1}, on all four lay-ups, Table 4. The similarity in the kinetic energy loss is striking, with laminates of similar $\bar{\theta}$ exhibiting very similar values of U_{loss}. Even comparing laminates of high and low $\bar{\theta}$ only contributes between a quarter to a third more to the dissipation.

Table 4: Incident (V_i) and residual (V_r) velocities for high-speed impact tests, and energy loss (U_{loss}) in the impact. U_i is the incident kinetic energy.

	$\bar{\theta}$	V_i	V_r	U_{loss}	U_{loss}/U_i
	–	m s^{-1}	m s^{-1}	J	–
UD	0	490	440	192	.19
Helicoid	0.04	450	392	202	.24
0°/90° – Heli.	0.96	466	390	269	.30
0°/90°	1	473	394	283	.31

This suggests that with sufficiently high velocity (and therefore pressure), the increased shear strength diminishes the influence of $\bar{\theta}$ on the dissipation capacity. Interestingly, the UD plate did not sustain any fibre fracture, while the Helicoid failed through fibre fracture in the front two-thirds of the plate and splitting through the remainder.

5. Optimal architecture design for V_L

In the present study, the investigation is restricted to two parameters by which the lay-up can be characterised: that of anisotropic ratio β, and the average angular off-set of adjacent plies $\bar{\theta}$. This section shall focus chiefly on these aspects, but comment shall also be made upon ply thickness and woven architectures.

Figure 4 maps out all possible combinations of architecture, and such architectures have been designed and tested that exist at the extrema of this space. Of these, the 0°/90° lay-up exceeded the other designs by a significant margin (74% over the 0°/90°– Helicoid). It is argued that the 0°/90° configuration (β= 0.5, $\bar{\theta}$= 1) is optimal.

Consider moving from this coordinate by a number of trajectories. Each is taken in turn and the expected properties of each new architecture discussed:

1. Vertically downward towards the 0°/90°– Helicoid lay-up. In order to move in the direction of decreasing β (becoming more isotropic), the addition of more fibre directions is required. Two consequences follow that reduce ballistic efficiency: first, the loading at the boundary is smaller, reducing pull-out; second, the additional fibre directions stiffen the laminate in-plane, giving greater resistance to scissoring and reducing the deflection.
2. Horizontally left (keeping $\beta = 0.5$). This is achieved by block stacking plies. For laminates of the form: $[0^\circ_m/90^\circ_m]_n$, m is increased whist n is decreased, keeping the product mn constant (refer to Fig. 4). Attwood et al. [3] have shown that the peak strengths of laminates decreased with increasing ply thickness. Small deviations from this coordinate will then reduce the indirect tension strength; very large deviations may transition into a splitting micro mechanism as $\bar{\theta}$ approaches zero.
3. Any trajectory in the quadrant bounded by (1) and (2) above. In this region, both β and $\bar{\theta}$ decrease with deviation from the 0°/90° coordinate, and since both are seen to have a detrimental effect, it follows that all lay-ups bounded in this region are sub-optimal.
4. Tracking along the boundary with unattainable space. This boundary is obtained by lay-ups of the form $[0^\circ/\theta^\circ]_{24}$ where θ takes a value between 0° and 90°. These lay-ups resemble helicoidal arrangements in that they exhibit a single offset angle, and as such the competition between the micro mechanisms of fibre-failure and splitting will be similar, suggesting a velocity dependence. However, these lay-ups are also highly anisotropic, so pull-out will certainly occur.
5. Trajectories bounded by (2) and (4). Similar to that seen in the Helicoid lay-up, large deviations from the 0°/90° coordinate are expected to split (either fully or partially), thus reducing the ballistic limit. Small deviations are likely to perform in a similar manner to the 0°/90°.

5.1. Weaves

Woven architectures help to further reduce the propensity for splitting, thus encouraging an indirect tension type of failure. However, the benefit of this is not clear since non-woven 0°/90° lay-ups show no indication of splitting in the present study. It is possible that this may change with sharp-nosed projectiles. Woven architectures also introduce a number of detrimental effects. Fibre tows are by nature wavy, and this aspect would be expected to have adverse effects upon macro mechanisms in at least 4 ways: (i) the total volume fraction of fibres would be reduced from that of a straight fibre ply, (ii) the longitudinal wave speed along the primary fibres would be reduced, thus reducing the fraction of the plate engaged in dissipation for a given velocity compared to a straight fibre

laminate, (iii) wave reflections at the cross overs amplifies fibre strain near the impact point [22], and (iv) under large shear strains woven architectures can 'lock-up', giving resistance to further scissoring.

6. Further design considerations

Systems such as the laminates investigated in the present study should be considered structures rather than materials. As such, the absolute plate dimensions are important, as are the specifics of the boundary condition. These parameters can have a first order effect upon the ballistic limit obtained in a given test. This poses implications for material validation tests, where test plates differ in size and boundary from the system being validated.

Plate size Pull-out occurs when the longitudinal waves are reflected from the edge of the plate, causing material to be drawn in. Small plates allow this pull-out to happen more quickly, such that there is greater dissipation prior to failure through a micro mechanism.

Boundary friction Boundary friction F_F is dependent on both the frictional coefficient and the normal force applied to the boundary (Equation 3), and has a direct bearing on the dissipation of energy at the boundary (Equation 6). However, too high a pressure will switch off pull-out altogether, too low and the plate will completely pull-out from the clamp support. Thus there follows that an optimum clamping pressure exists that maximises U_{PO}.

The present study has considered only hard spherical projectiles (i.e. those which are undeformable and blunt). The loading condition upon a plate will inevitably become more complex with the introduction of sharp-nosed projectiles, such geometries will likely favour splitting type mechanisms due to the wedging action of a projectile. Deformable projectiles (such as copper fragment simulating projectiles) tend to flatten, i.e. become more blunt, so may transition from a regime which favours splitting-type behaviours into a range of behaviours more closely matching the present study.

7. Conclusions

The design space of laminates is explored by the fabrication and testing of four lay-ups that lie at the four extremes of all possible configurations. The axes of this space are the average ply off-set angle and the anisotropy denoted $\bar{\theta}$ and β respectively, and defined in Equations (1–2).

- The macro mechanisms that operate under impact relate to the plate anisotropy β. High values of β correspond to significant pull-out and scissoring, and low values to much lower pull-out displacements and wrinkling close to the boundary.
- The micro mechanisms that operate under impact relate to the average ply off-set angle $\bar{\theta}$. High values of $\bar{\theta}$ correspond to fibre-failure (indirect tension), whereas low values promote splitting.
- Pull-out has a first order effect upon the ballistic limit V_L. In the 0°/90° laminate at 400 m s^{-1}, the estimated work done at the boundary was nearly three-quarters of the total kinetic energy of the projectile. This has significant implications for computational models that seek to capture the V_L. Such models will, in some way, need to account for boundary effects.
- Inter- and intra- laminar shear are important global mechanisms that enable pull-out. These shear mechanisms in themselves may not contribute significantly to energy dissipation; however, these mechanisms are essential for pull-out to occur.
- Geometries with a small $\bar{\theta}$ (i.e. the Helicoid), show a transitioning behaviour from fibre failure to splitting. At high velocities, fibre failure is switched on (high pressure elevates shear strength), and at low velocities, splitting occurs (shear strength drops with pressure drop).
- 0°/90° lay-ups are optimised for penetration resistance. However, when considering other design metrics (such as back face deflection) isotropic lay-ups such as the 0°/90°– Helicoid show promise. More detailed analysis is required to find optimal geometries that balance these two metrics.

Data

High speed imaging data is available for down load at the following repository: https://www.repository.cam.ac.uk/handle/1810/250407

Acknowledgements

The authors wish to thank DSM Dyneema for supplying material for the construction of laminate plates. Dyneema® is a trademark of DSM. Dr B. P. Russell was supported by a Ministry of Defence / Royal Academy of Engineering Research Fellowship. The authors are also appreciative of technical insight provided by Dr. O'Masta.

References

[1] Karthikeyan, K., Russell, B.P., Fleck, N.A., O'Masta, M., Wadley, H.N.G., Deshpande, V.S.. The soft impact response of composite laminate beams. Int J Impact Eng 2013;60:24–36. doi: 10.1016/j.ijimpeng.2013.04.002.

[2] Nazarian, O., Zok, F.W.. Constitutive model for the shear response of Dyneema® fiber composites . Composites Part A: Applied Science and Manufacturing 2014;66:73–81. doi: 10.1016/j.compositesa.2014.06.012.

[3] Attwood, J.P., Khaderi, S.N., Karthikeyan, K., Fleck, N.A., O'Masta, M.R., Wadley, H.N.G., et al. The out-of-plane compressive response of Dyneema® composites. Journal of the Mechanics and Physics of Solids 2014;70:200–226. doi: 10.1016/j.jmps.2014.05.017.

[4] O'Masta, M., Crayton, D., Deshpande, V., HNG, W.. Mechanisms of penetration in polyethylene reinforced cross-ply laminates. Accepted for publication in the International Journal of Impact Engineering 2015;doi: 10.1016/j.ijimpeng.2015.08.012.

[5] Chocron, S., Nicholls, A.E., Brill, A., Malka, A., Namir, T., Havazelet, D., et al. Modeling unidirectional composites by bundling fibers into strips with experimental determination of shear and compression properties at high pressures. Composites Science and Technology 2014;101:32–40. doi: 10.1016/j.compscitech.2014.06.016.

[6] Heckert, W.W.. Laminated armor plate structure. 1946. US Patent 2,399,184; page 2, column 1, lines 28-31.

[7] Rose, A., Merrett, G.J.. Armor. 1951. US Patent 2,562,951; column 3, lines 70-74.

[8] Simmelink, J., Mencke, J., Marissen, R., Jacobs, M.. Process for making high-performance polyethylene multifilament yarn. 2011. EP Patent 1,699,954.

[9] Vargas-Gonzalez, L., Walsh, S.M., Wolbert, J.. Impact and ballistic response of hybridized thermoplastic laminates. Army Research Laboratory 2011;ARL-MR-0769.

[10] Vargas-Gonzalez, L., Gurganus, J.. Influence of composite architecture on stress transmittance in ultra-high molecular weight polyethylene composite armor. In: Ballistics 2014: Proceedings of the 28th International Symposium on Ballistics; vol. 2. DEStech Publications; 2014, p. 1652–1662.

[11] Zhang, T.G., Satapathy, S.S., Vargas-Gonzalez, L.R., Walsh, S.M.. Ballistic impact response of ultra-high-molecular-weight polyethylene (uhmwpe). Composite Structures 2015;133:191–201. doi: 10.1016/j.compstruct.2015.06.081.

[12] Wang, Y., Chen, X., Young, R., Kinloch, I., Garry, W.. An experimental study of the effect of ply orientation on ballistic impact performance of multi-ply fabric panels. Textile Research Journal 2015;doi: 10.1177/0040517514566110.

[13] Apichattrabrut, T., Ravi-Chandar, K.. Helicoidal composites. Mechanics of Advanced Materials and Structures 2006;13(1):61–76. doi: 10.1080/15376490500343808.

[14] Grunenfelder, L., Suksangpanya, N., Salinas, C., Milliron, G., Yaraghi, N., Herrera, S., et al. Bio-inspired impact-resistant composites. Acta Biomaterialia 2014;10(9):3997–4008. doi: 10.1016/j.actbio.2014.03.022.

[15] Attwood, J., Russell, B.P., Fleck, N., Deshpande, V.. Mechanisms of the penetration of ultra-high molecular weight polyethylene composite beams. Submitted for publication in the International Journal of Impact Engineering 2015;:.

[16] Russell, B.P., Karthikeyan, K., Deshpande, V.S., Fleck, N.A.. The high strain rate response of Ultra High Molecular-weight Polyethylene: From fibre to laminate. Int J Impact Eng 2013;60:1–9. doi: 10.1016/j.ijimpeng.2013.03.010.

[17] Karthikeyan, K., Russell, B., Fleck, N., Wadley, H., Deshpande, V.. The effect of shear strength on the ballistic response of laminated composite plates. European Journal of Mechanics - A/Solids 2013;42(0):35–53. doi: 10.1016/j.euromechsol.2013.04.002.

[18] Karthikeyan, K., Russell, B.P., Deshpande, V.S., Fleck, N.A.. Multi-hit armour characterisation of metal-composite bi-layers. J Mech Mater Struct 2012;7(7):721–734. doi: 10.2140/jomms.2012.7.721.

[19] Porter, F.C.. Zinc Handbook: Properties, Processing, and Use In Design. CRC Press; 1991.

[20] Gilmore, J., Stenvers, D., Chou, R.. Some recent developments of rope technologies - further enhancements of high performance ropes. In: Oceans. 2008, p. 1–7. doi: 10.1109/OCEANS.2008.5151814.

[21] Maxwell, J.C.. On the calculation of the equilibrium and stiffness of frames. Philosophical Magazine 1864;27:294–299.

[22] Roylance, D.. Stress wave propagation in fibres: Effect of crossovers. Fibre Science and Technology 1980;13(5):385–395. doi: 10.1016/0015-0568(80)90011-1.